Letter

Non-Hermitian topology and skin modes in the continuum via parametric processes

Markus Bestler ,[1,*] Alexander Dikopoltsev ,[2] and Oded Zilberberg [1,†]
[1]*Department of Physics, University of Konstanz, 78464 Konstanz, Germany*
[2]*Institute for Quantum Electronics, ETH Zurich, CH-8093 Zürich, Switzerland*

(Received 28 May 2025; revised 19 September 2025; accepted 8 June 2026; published 20 August 2026)

We demonstrate that Hermitian, nonlocal parametric pairing processes can induce non-Hermitian topology and skin modes in the continuum, offering a simple alternative to complex bath engineering. Our model, stabilized by local dissipation reveals exceptional points that spawn a tilted non-Hermitian Fermi arc in the dispersion. Local dissipation prevents instabilities, while a bulk anomaly signals unscreened current response. Upon opening the boundaries, we observe a non-Hermitian skin effect with localized edge modes. Through bulk winding indices and non-Bloch theory, we establish a robust bulk-boundary correspondence, highlighting parametric drives as a scalable route to non-Hermitian topology in bosonic continuum systems.

DOI: 10.1103/yhkx-tn6l

Topological phases of matter constitute a remarkable class of systems whose physical behavior is governed not by local order parameters but by global, quantized invariants [1–7]. These topological indices characterize the bulk band structure and dictate quantized response functions, such as conductance, which are therefore immune to disorder and other local perturbations. Crucially, the robustness of these responses is often tied to the presence of anomalies, i.e., violation of conservation laws [8]. At interfaces between topologically distinct media, such as between a nontrivial phase and the vacuum, these anomalies manifest in robust boundary phenomena including gapless edge modes or fractionalized excitations. Prominent examples include the quantum Hall effect [1,9], where the Hall conductance is quantized by a Chern number; topological insulators, protected by time-reversal symmetry [4,5]; high-order topological insulators associated with topology from higher dimensions than that of the system [2,10–14]; and even topological phases in quasiperiodic systems [15–17].

In recent years, the study of non-Hermitian (NH) topological systems has uncovered a wealth of phenomena in open and dissipative settings, where energy is not conserved and systems are described via effective NH Hamiltonians [18–21]. In these systems, conventional topology must be reconsidered: Spectra are generally complex, eigenstates lose orthogonality, and boundary sensitivity increases significantly. A striking example is the NH skin effect (NHSE), where many bulk eigenstates localize at system edges, defying Hermitian bulk-boundary expectations [22–25]. This signals a breakdown of standard topological principles and calls for refined theoretical approaches, e.g., adaptation of topological winding numbers to the complex energy plane [26–29]. Similarly, non-Bloch band theory further addresses the breakdown of Bloch's theorem by introducing a generalized Brillouin zone with complex momenta, thereby restoring a modified bulk-boundary correspondence [30–33]. Together, these tools allow a systematic understanding of NH topology and edge behavior.

Non-Hermitian topology has been demonstrated in diverse platforms by coupling lattice systems to engineered environments. A central feature in many is the presence of exceptional points, where eigenvalues and eigenvectors coalesce, often causing instabilities unless finite mode lifetimes are introduced. To address this, most realizations use tight-binding lattice models and complex bath engineering. In cold atom setups, loss is induced via coupling to untrapped states or near-Feshbach resonances [34,35]. Photonic systems use gain and absorption to enable topological lasing [36–39], directional amplification, and nonreciprocal transport [40–43]. Electronic circuits implement asymmetric couplings using resistors and amplifiers [44], while mechanical and acoustic systems achieve similar effects through damping or motor-driven elements [45]. Despite these advances, reliance on engineered baths remains a key challenge, motivating the search for more natural and scalable approaches.

Parametric driving offers a powerful route to engineer effective interactions and dissipation in quantum systems [46]. Typically realized through two-photon (or two-mode) processes, such drives can induce squeezing, implement coherent pairing terms, or mimic effective damping, all while preserving Hermitian dynamics. By tuning the drive amplitude and frequency, these systems can reach exceptional points, beyond which time-translation symmetry-breaking bifurcations emerge. Such instabilities are often stabilized and postponed by local dissipation [47]. These features make parametric drives especially valuable in systems where direct coupling or dissipation control is challenging. Prominent applications include parametric amplifiers (paramps) for quantum-limited

*Contact author: markus.bestler@uni-konstanz.de
†Contact author: oded.zilberberg@uni-konstanz.de

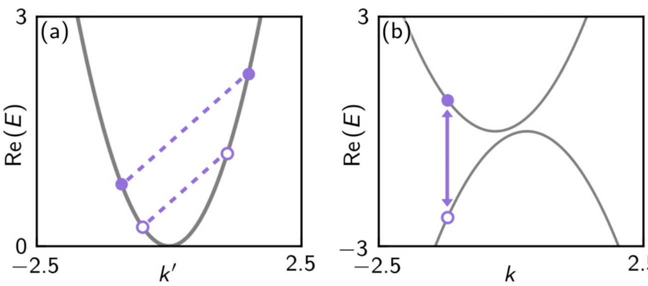

FIG. 1. Model. (a) Sketch of the model [cf. Eq. (1)]: Bosonic particles with a parabolic dispersion (gray line) are created (annihilated) in pairs with opposite momentum plus a momentum shift $2k_0$, e.g., marked by full (empty) purple circles connected by dashed lines. This also leads to an energy shift between created (annihilated) particle pairs. (b) The dynamical matrix of the system over a shifted momentum Nambu spinor [cf. Eq. (2)]. Here, the pair creation (annihilation) appear as a particle-hole scattering with a shifted momentum. We use $k_0 = 0.3$.

signal readout [48], optomechanical sensors with enhanced sensitivity [49], Kerr parametric oscillators used in quantum information processing [50], and Ising annealers [51–53]. In recent years, parametric processes, or equivalently squeezing, were found to provide a promising platform for NH topology and NHSEs on lattices [54–57], enabling, for example, a bosonic analogue of the Kitaev chain [58–60], and anomalous bulk-boundary correspondences [61].

In this work, we demonstrate that Hermitian, nonlocal parametric pairing processes can give rise to NH topology and skin modes in the continuum. Crucially, this is accomplished without relying on complicated bath engineering. Specifically, our model is stabilized by simple local dissipation and operates free from any underlying lattice structure. We begin by analyzing the bulk of the continuum system, where the parametric drive leads to level attraction between particle and hole branches. Beyond a critical threshold, exceptional points emerge and form a non-Hermitian Fermi arc in the dispersion. We introduce local dissipation to stabilize the system, preventing dynamical instabilities. We then identify a bulk anomaly that signals an unscreened current response, hinting at anomalous boundary behavior. Indeed, upon opening the boundaries, we observe a clear NHSE with strongly localized edge modes. We quantify this behavior using a bulk winding index and complete the topological characterization using non-Bloch band theory, which restores a consistent bulk-boundary correspondence for our continuum-driven model. Our approach is broadly applicable, as (1) many relevant platforms are inherently continuous rather than lattice based, (2) our mechanism maps to the experimental demonstration in Ref. [62], and (3) it requires minimal fine-tuning or external engineering, underscoring its generality.

We consider a continuum one-dimensional bosonic model with momentum-shifted particle pair production [see Fig. 1(a)]

$$H = \int dk' \left[\frac{k'^2}{2m} a^\dagger_{k'} a_{k'} + \frac{g}{2} \left(a^\dagger_{k'} a^\dagger_{-k'+2k_0} + \text{H.c.} \right) \right]. \qquad (1)$$

The particles have a parabolic dispersion as a function of wave number k', and we use units where $\hbar = 1$. For simplicity, we set $m = 1/2$. The bosonic annihilation operator $a_{k'}$ removes a particle from mode k'. Pairs of particles are created (annihilated) in a parametric process with amplitude g, involving opposing momenta alongside a momentum shift of $2k_0 \in \mathbb{R}$, akin to finite-momentum Cooper pairs [63]. It is comfortable, henceforth, to shift the momentum origin to $k' = k + k_0$. Thus, we can rewrite Eq. (1) on top of a shifted momentum bosonic Nambu spinor $\mathbf{a}_k = (a_{k+k_0}, a^\dagger_{-k+k_0})^T$ with an associated Hamiltonian $H = \frac{1}{2} \int dk\, \mathbf{a}^\dagger_k \mathbf{H}_k \mathbf{a}_k$, where $\mathbf{H}_k$ is a 2×2 Hamiltonian density. In order to diagonalize the model, we write the corresponding dynamical matrix [64]

$$\mathbf{D}_k \equiv \sigma_z \mathbf{H}_k = \begin{pmatrix} (k+k_0)^2 & g \\ -g & -(-k+k_0)^2 \end{pmatrix}, \qquad (2)$$

where σ_z is a Pauli matrix. Here, the pair creation (annihilation) maps to a particle-hole scattering process [see Fig. 1(b)].

The resulting spectrum reads $E = 2kk_0 \pm \sqrt{(k^2 + k_0^2)^2 - g^2}$ [see Figs. 2(a)–2(f)]. For $g = 0$, we find free parabolic particle and hole dispersions with an indirect gap, due to the shifted momentum labeling. The parametric particle-hole scattering causes level attraction [65]. We observe three regimes: (1) For $k_0 = 0$ and $g \neq 0$, no momentum shift is present. Due to level attraction, particle and hole bands coalesce for $|k| < \sqrt{|g|}$, forming a continuous horizontal non-Hermitian Fermi arc [19] with broken PT-symmetry [66] ending in two exceptional points [see Fig. 2(a)]. On this arc, $\text{Im}(E)$ splits into branches with lifetimes $\text{Im}(E) \lesssim 0$, marking parametric instabilities [see Fig. 2(b)]. (2) For finite $|k_0| < \sqrt{|g|}$, the non-Hermitian Fermi arc persists for $|k| < \sqrt{|g| - k_0^2}$ [see Fig. 2(c)], and tilts due to the momentum shift. In the spectrum, the branches with nonzero $\text{Im}(E)$ form two closed loops [see Fig. 2(d)]. (3) Increasing k_0 further until $|k_0| > \sqrt{|g|}$, the momentum shift dominates the level attraction, reopening the indirect gap as in the noninteracting case [see Fig. 2(e)]. The non-Hermitian Fermi arc disappears and the free dispersion is only marginally affected. All eigenenergies are purely real [see Fig. 2(f)]. As the level attraction produces a non-Hermitian Fermi arc pertaining to modes with negative lifetimes [$\text{Im}(E) > 0$] [see Figs. 2(b) and 2(d)], the system would become unstable whenever the Fermi arc appears. To stabilize the effect, we introduce uniform local damping of strength γ. Note that this damping solely stabilizes the system's modes without impacting its non-Hermitian topology. Only now, the system is described by a non-Hermitian Hamiltonian $\tilde{H} = H - i\gamma \int dk' a^\dagger_{k'} a_{k'}$ and corresponding dynamical matrix $\tilde{\mathbf{D}}_k = \sigma_z \mathbf{H}_k - i\gamma \mathbb{1}$. In a physical system, we require $\gamma \geqslant \sqrt{g^2 - k_0^4}$ to ensure positive lifetimes for all modes and stabilize the system.

As the scattering particles and holes are shifted in momentum, the non-Hermitian Fermi arc is tilted, i.e., $d[\text{Re}(E)]/dk \neq 0$ for $k_0 \neq 0$. In a Hermitian system, this would imply that these modes have a finite group velocity; i.e., these modes contribute to a finite probability current. To study whether this behavior extends to the NH case, we use the

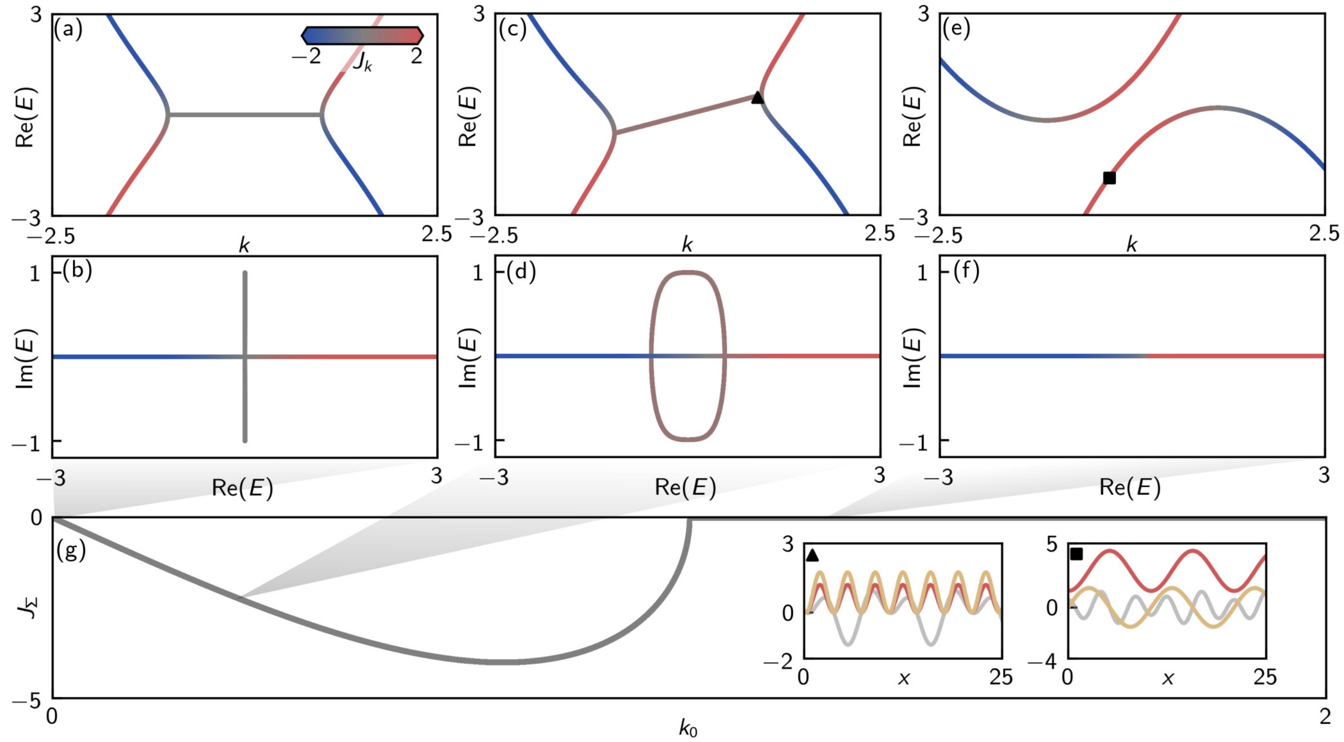

FIG. 2. Bulk spectrum and anomaly. (a), (c), (e) Dispersion relation, Re(E), as a function of the shifted momentum k, for $\gamma = 0$, $g = 1$, and $k_0 = 0, 0.3, 1.2$, respectively. Modes are colored according to the probability current J_k [cf. Eq. (3)]. (b), (d), (f) Spectral plot of lifetime $\mathrm{Im}(E)$ as a function of $\mathrm{Re}(E)$ for the same parameters and coloring as in panels (a), (c), and (e), respectively. (g) Total current of modes not participating in the non-Hermitian Fermi arc, J_Σ, as a function of the momentum shifts k_0. Insets: $\mathrm{Re}(\langle\psi_x\rangle)$ (gray), probability current J (red), and interaction-generated sink/source term (yellow) in real space [cf. Eq. (3)] corresponding to the modes at the positions marked with a triangle in panel (c) and square in panel (e).

mean-field limit of the Lindblad master equation corresponding to our NH model $\tilde{H}$ [67] to calculate the time evolution of the mean-field density $\rho = \langle\psi_x^\dagger\rangle\langle\psi_x\rangle$

$$\partial_t \rho = -\partial_x J - 2\gamma\rho - 2g\mathrm{Im}(e^{-2ik_0x}\langle\psi_x\rangle^2), \tag{3}$$

where $\psi_x = (1/\sqrt{2\pi})\int dk e^{ikx} a_k$ is the local bosonic field operator at position x, and the closed system probability current reads $J = i[(\partial_x\langle\psi_x^\dagger\rangle)\langle\psi_x\rangle - (\partial_x\langle\psi_x\rangle)\langle\psi_x^\dagger\rangle]$. Compared with the standard Hermitian continuity equation, Eq. (3) features additional sink and source terms. An obvious sink arises due to the uniform damping, $2\gamma\rho$. The term arising due to the parametric pair production, $\propto \mathrm{Im}(e^{-2ik_0x}\langle\psi_x\rangle^2)$, acts as a spatially dependent sink or source, depending on the spatial structure of $\langle\psi_x\rangle$ corresponding to a mode k (see insets of Fig. 2).

The contribution from the local sinks and sources, arising from the pairing term, averages out for modes that are not part of the non-Hermitian Fermi arc, namely, when integrating over distances in space much larger than the periodicity of the wave function. Hence, for long length scales, these modes experience the same density loss. It is instructive to define J_Σ as the total average current arising from these modes [see Fig. 2(g)]. In the case of weak coupling, $\sqrt{|g|} < |k_0|$, we have no non-Hermitian Fermi arc, and $J_\Sigma = \int_{-\infty}^{\infty} J_k dk$ sums over the current J_k arising from all modes of the system. In this limit, every mode in the system has a counterpropagating mode [see Fig. 2(e)], regardless of the choice of the global damping γ, such that $J_\Sigma = 0$. Instead, when the non-Hermitian Fermi arc appears, $\sqrt{|g|} > |k_0|$, we have $J_\Sigma = \int_{-\infty}^{-\sqrt{|g|-k_0^2}} J_k dk + \int_{\sqrt{|g|-k_0^2}}^{\infty} J_k dk \neq 0$, which may be understood as an anomaly that must be screened by the modes in the non-Hermitian Fermi arc. Indeed, as long as the non-Hermitian Fermi arc is tilted, its modes transport a finite probability current [see Fig. 2(c)]. However, as $\mathrm{Im}(e^{-2ik_0x}\psi^2)$ does not average out over space for these modes, they experience additional sink or source terms [see insets of Fig. 2(g)]. Their transported current therefore changes relative to the other modes' currents over time. As a result, modes on the non-Hermitian Fermi arc cannot act as counterpropagating modes that screen the nonvanishing $J_\Sigma \neq 0$, leading to a persistent bulk current caused by the Hermitian parametric process [29,68]. Thus, we obtain a true anomaly in the bulk due to the tilt of the non-Hermitian Fermi arc, which requires a corresponding boundary effect that will cancel the unscreened current in the bulk [8,69]. Such bulk-boundary correspondence implies that when open boundary conditions are applied, boundary modes must appear in the system.

To confirm the formation of boundary modes, we Fourier transform the dynamical matrix $\tilde{\mathbf{D}}_k$ to real space, and then discretize it and diagonalize the finite system numerically [67]; see the eigenvalues of such a system in the upper left inset in Fig. 3(a). Note that the discretized version of our model takes a similar form as the Bosonic Kitaev chain [58,67]. We ascribe a wave number to each finite system mode by

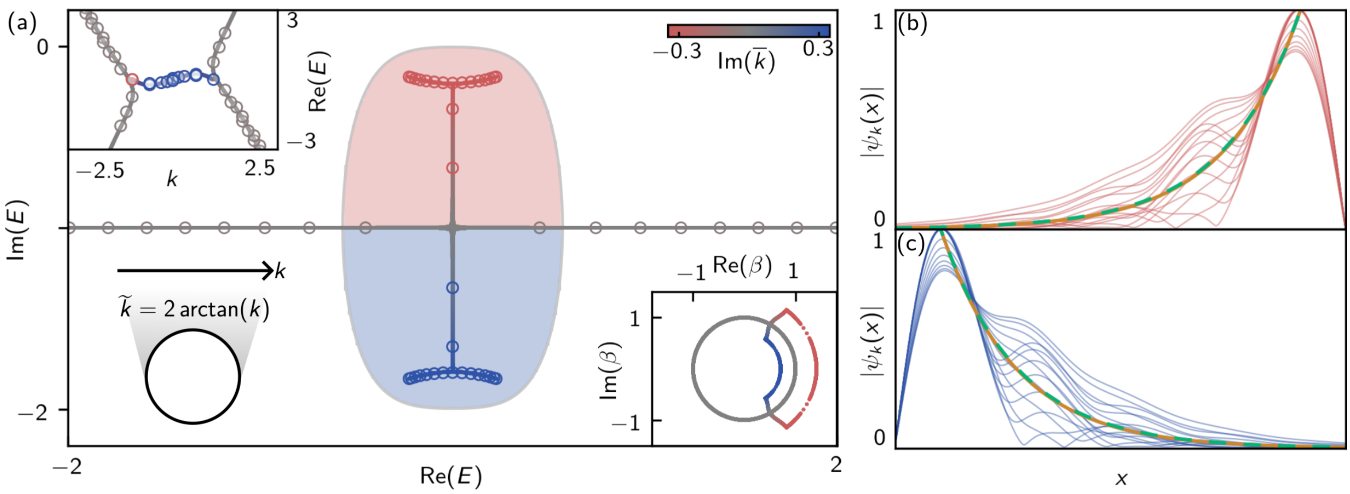

FIG. 3. Bulk-boundary correspondence. Spectral plot as in Fig. 1(d) for $k_0 = 0.3$ and $g = \gamma = 1$ calculated numerically for a system with open boundary conditions (empty circle markers) and via non-Bloch theory (full markers). Modes localized on the left (right) edge are colored red (blue). Delocalized modes are colored gray. Colors of the non-Bloch theory calculation correspond to $\mathrm{Im}(\bar{k})$. Areas marked in light red (light blue) correspond to energies with a spectral winding number of -1 $(+1)$ [cf. Eq. (4)]. Energies outside of these two areas have spectral winding number 0. Insets (counterclockwise, starting from top left): dispersion relation calculated numerically [cf. Fig. 1(c)] (empty circle markers) and via non-Bloch theory (full markers); illustration of how the continuous bulk momentum, k, can be compactified to a periodic momentum $\tilde{k}$ by mapping it to a circle via $\tilde{k} = 2\arctan(k)$; and generalized Brillouin zone of the model in terms of the non-Bloch factor β. (b) Local density of numerically calculated finite-frequency skin modes on the right edge of the open system (red) and exponential $e^{\mathrm{Im}(\bar{k}_l)(x-x_0)}$ with the localization $\mathrm{Im}(k_l)$ of the most (orange, $\mathrm{Im}(\bar{k}_l) \approx 0.345$) and the least (green dashed, $\mathrm{Im}(\bar{k}_l) \approx 0.339$) localized finite frequency skin modes. (c) Same as in panel (b) for the left edge of the system.

Fourier transforming it and picking the highest amplitude Fourier component as k. The resulting dispersion relation [Fig. 3(a)] has a similar structure as the bulk continuous model [cf. Fig. 1(c)]. Unlike the bulk model, however, the complex energy spectrum at the non-Hermitian Fermi arc forms two arches with $\mathrm{Im}(E) \lessgtr -\gamma$ instead of closed loops [cf. Figs. 3(a) and 2(d)], respectively. Moreover, the modes with $\mathrm{Im}(E) > -\gamma$ $[\mathrm{Im}(E) < -\gamma]$ are exponentially localized at the right (left) boundary of the system for $k_0 > 0$; see, e.g., numerically calculated modes in Figs. 3(b) and 3(c).

The accumulation of a large number of modes near the boundaries and the strong sensitivity of the energy spectrum to boundary conditions is an NHSE. Crucially, in this work, the NHSE arises from the Hermitian coupling between momentum-shifted particle and hole modes, which gives rise to the tilted non-Hermitian Fermi arc; the NH damping only ensures a positive lifetime for all modes. The NHSE has a topological origin that can be classified via a spectral winding number [26,27]

$$W(E) = \int_{-\pi}^{\pi} \frac{d\tilde{k}}{2\pi i} \frac{d}{d\tilde{k}} \ln(\det(\tilde{\mathbf{D}}_{\tilde{k}}(\tilde{k}) - \mathbb{1}E)), \tag{4}$$

for periodic tight-biding systems with a Brillouin zone $\tilde{k} \in [-\pi, \pi]$, where $E \in \mathbb{C}$ is a complex energy, and $W(E) < 0$ $[W(E) > 0]$ implies boundary modes on the right (left) side of the system. In our continuum model (1), $k \in (-\infty, \infty)$. To apply the spectral winding number, we compactify momentum space using $\tilde{k} = 2\arctan(k)$, and wrap $-\infty$ onto ∞ to obtain a periodic structure [70] [see Fig. 3(a), bottom left]. This approach guarantees a well-quantized topological index, as the system approaches the continuum limit, $k \to \pm\infty$. Calculating the winding number for every $E \in \mathbb{C}$ reveals that the non-Hermitian Fermi arc engenders two regions with $W(E) = \pm 1$ separated by a line at $\mathrm{Im}(E) = -\gamma$ [see Fig. 3(a)]. We thus find the topological index classifying the bulk anomaly presented in Fig. 2(g). Note that the spectral point gap, which gives rise to the nontrivial winding number, arises due to the tilt of the non-Hermitian Fermi arc [see Figs. 2(a)–2(d)].

The spectral winding number [Eq. (4)] predicts localized skin modes in a semi-infinite system. In Fig. 3, we see that the system with open boundary conditions on both ends of the chain exhibits skin modes. To prove the NH bulk-boundary correspondence in the finite model, we use non-Bloch theory [30,32]. This approach also allows us to analytically describe the localization lengths of the skin modes. To apply non-Bloch theory, we replace the real wave number k in Eq. (2) with a complex wave number $\bar{k} \in \mathbb{C}$. Here, $\mathrm{Im}(\bar{k})$ describes the spatial localization of a mode. To select the modes that satisfy the open boundary conditions, we first solve the non-Bloch equation

$$\det(\tilde{\mathbf{D}}_{\bar{k}} - \mathbb{1}E) = 0 \tag{5}$$

for every $E \in \mathbb{C}$. We obtain a fourth-order polynomial equation in $\bar{k}$, which has four solutions $\bar{k}_j$ with $j \in \{1, 2, 3, 4\}$ for every E. We sort the solutions such that $\mathrm{Im}(\bar{k}_j) \leqslant \mathrm{Im}(\bar{k}_{j+1})$. The non-Bloch condition states that modes $\bar{k}_2$ and $\bar{k}_3$ fulfill the open boundary conditions, if and only if $\mathrm{Im}(\bar{k}_2) = \mathrm{Im}(\bar{k}_3)$. For modes $\bar{k}_1$ and $\bar{k}_4$, $\mathrm{Im}(\bar{k}_1) = \mathrm{Im}(\bar{k}_2) = \mathrm{Im}(\bar{k}_3) = \mathrm{Im}(\bar{k}_4)$ have to hold to fulfill the open boundary conditions. The collection of all $\bar{k}$ satisfying this requirement constitutes the generalized Brillouin zone. Commonly, the generalized Brillouin zone is visually represented in terms of the non-Bloch factor $\beta = \exp(i\bar{k})$ [see bottom right inset of Fig. 3(a)]. In our case, it takes the form of a unit circle, with additional sections at the non-Hermitian Fermi arc. Here, the generalized Brillouin zone splits up into two arcs corresponding to the modes localized on the different edges of the system. Using Eq. (5), we also find the open boundary energy spectrum of the model [see Fig. 3(a)]. The exact spectrum coincides with the numerical one. In the top left inset of Fig. 3(a), we draw the obtained dispersion relation, which is in agreement with the numerical solutions.

Having applied non-Bloch theory to our model, we use it to analytically determine the localization $|\mathrm{Im}(\bar{k})|$ of the skin modes [see Figs. 3(b) and 3(c)]. The non-Bloch equation (5) is a fourth-order polynomial that is solvable, but its roots must also satisfy the non-Bloch condition, making a full analytical treatment nontrivial. We focus on finite-frequency modes with the highest and lowest $|\mathrm{Im}(\bar{k})|$; details on zero-frequency modes are provided in Ref. [67]. The most localized finite-frequency modes occur for $\mathrm{Re}(E) \to 0$, where the non-Bloch equation and condition reduce to a third-order polynomial in $\mathrm{Im}(\bar{k})^2$. Solving it gives an analytical expression for $\mathrm{Im}(\bar{k})$; for $g = \gamma = 1$ and $k_0 = 0.3$, we find $|\mathrm{Im}(\bar{k})| \approx 0.345$, as shown in Figs. 3(b) and 3(c). For $|k_0/\sqrt{|g|}| \lesssim 0.35$, the least localized modes fulfill the non-Bloch condition via a double zero, i.e., $\bar{k}_2 = \bar{k}_3$, not just matching imaginary parts. We then use the discriminant of Eq. (5) and solve a resulting quartic analytically. At $g = \gamma = 1$ and $k_0 = 0.3$, this gives $|\mathrm{Im}(\bar{k})| \approx 0.339$. We find identical localization strengths on both edges. This analytical treatment completes the demonstration of the NH bulk-boundary correspondence in our system.

We introduced a continuum model that exhibits topological skin modes arising from nonlocal parametric processes. This mechanism, fundamentally distinct from conventional bath-engineered NHSE models, enables the realization of directional localization in systems lacking lattice periodicity. Our framework is broadly applicable to a variety of bosonic platforms [67], such as magnomechanical systems [71] and continuous exciton-polariton systems [55,72]. Moreover, it was recently realized on top of a nonlinear steady state in a mode-locked quantum cascade laser [62], where topology was realized on ultrafast timescales. Future work will explore how strong interactions modify and enrich the topological structure of the model.

We are grateful for fruitful discussions with J. del Pino, B. Schneider, and J. Faist. We acknowledge funding from the Deutsche Forschungsgemeinschaft (DFG) via Projects No. 449653034 (Heisenberg), No. 425217212 (SFB1432), No. 521530974 (FOR5688), No. 545605411 (ANR), as well as from the Swiss National Science Foundation (SNSF) through the Sinergia Grant No. CRSII5_206008/1 and ETH Fellowship program 22-1 FEL-46 to AD.

Data availability. There are no publicly available research data or software supporting this manuscript. Requests for further information or data should be sent to the authors.

[1] D. J. Thouless, M. Kohmoto, M. P. Nightingale, and M. den Nijs, Quantized Hall conductance in a two-dimensional periodic potential, Phys. Rev. Lett. **49**, 405 (1982).

[2] R. Resta and D. Vanderbilt, Theory of polarization: A modern approach, in *Physics of Ferroelectrics: A Modern Perspective* edited by K. Rabe, C. H. Ahn, and J.-M. Triscone (Springer, Berlin, Heidelberg, 2007), pp. 31–68.

[3] D. Xiao, M.-C. Chang, and Q. Niu, Berry phase effects on electronic properties, Rev. Mod. Phys. **82**, 1959 (2010).

[4] M. Z. Hasan and C. L. Kane, *Colloquium*: Topological insulators, Rev. Mod. Phys. **82**, 3045 (2010).

[5] X.-L. Qi and S.-C. Zhang, Topological insulators and superconductors, Rev. Mod. Phys. **83**, 1057 (2011).

[6] B. A. Bernevig, *Topological Insulators and Topological Superconductors* (Princeton University Press, Princeton, 2013).

[7] T. Ozawa, H. M. Price, A. Amo, N. Goldman, M. Hafezi, L. Lu, M. C. Rechtsman, D. Schuster, J. Simon, O. Zilberberg, *et al.*, Topological photonics, Rev. Mod. Phys. **91**, 015006 (2019).

[8] J. Fröhlich, Gauge invariance and anomalies in condensed matter physics, J. Math. Phys. **64**, 031903 (2023).

[9] K. V. Klitzing, G. Dorda, and M. Pepper, New method for high-accuracy determination of the fine-structure constant based on quantized Hall resistance, Phys. Rev. Lett. **45**, 494 (1980).

[10] J. C. Teo and C. L. Kane, Topological defects and gapless modes in insulators and superconductors, Phys. Rev. B **82**, 115120 (2010).

[11] Y. E. Kraus, Z. Ringel, and O. Zilberberg, Four-dimensional quantum Hall effect in a two-dimensional quasicrystal, Phys. Rev. Lett. **111**, 226401 (2013).

[12] W. A. Benalcazar, B. A. Bernevig, and T. L. Hughes, Quantized electric multipole insulators, Science **357**, 61 (2017).

[13] I. Petrides, H. M. Price, and O. Zilberberg, Six-dimensional quantum Hall effect and three-dimensional topological pumps, Phys. Rev. B **98**, 125431 (2018).

[14] I. Petrides and O. Zilberberg, Higher-order topological insulators, topological pumps and the quantum Hall effect in high dimensions, Phys. Rev. Res. **2**, 022049(R) (2020).

[15] Y. E. Kraus, Y. Lahini, Z. Ringel, M. Verbin, and O. Zilberberg, Topological states and adiabatic pumping in quasicrystals, Phys. Rev. Lett. **109**, 106402 (2012).

[16] M. Verbin, O. Zilberberg, Y. Lahini, Y. E. Kraus, and Y. Silberberg, Topological pumping over a photonic Fibonacci quasicrystal, Phys. Rev. B **91**, 064201 (2015).

[17] O. Zilberberg, Topology in quasicrystals, Opt. Mater. Express **11**, 1143 (2021).

[18] Y. Ashida, Z. Gong, and M. Ueda, Non-Hermitian physics, Adv. Phys. **69**, 249 (2020).

[19] E. J. Bergholtz, J. C. Budich, and F. K. Kunst, Exceptional topology of non-Hermitian systems, Rev. Mod. Phys. **93**, 015005 (2021).

[20] F. Roccati, G. M. Palma, F. Ciccarello, and F. Bagarello, Non-Hermitian physics and master equations, Open Syst. Inf. Dyn. **29**, 2250004 (2022).

[21] V. M. Martinez Alvarez, J. E. Barrios Vargas, and L. E. F. Foa Torres, Non-Hermitian robust edge states in one dimension: Anomalous localization and eigenspace condensation at exceptional points, Phys. Rev. B **97**, 121401(R) (2018).

[22] N. Hatano and D. R. Nelson, Localization transitions in non-Hermitian quantum mechanics, Phys. Rev. Lett. **77**, 570 (1996).
[23] S. Yao and Z. Wang, Edge states and topological invariants of non-Hermitian systems, Phys. Rev. Lett. **121**, 086803 (2018).
[24] F. K. Kunst, E. Edvardsson, J. C. Budich, and E. J. Bergholtz, Biorthogonal bulk-boundary correspondence in non-Hermitian systems, Phys. Rev. Lett. **121**, 026808 (2018).
[25] C. H. Lee and R. Thomale, Anatomy of skin modes and topology in non-Hermitian systems, Phys. Rev. B **99**, 201103(R) (2019).
[26] D. S. Borgnia, A. J. Kruchkov, and R.-J. Slager, Non-Hermitian boundary modes and topology, Phys. Rev. Lett. **124**, 056802 (2020).
[27] N. Okuma, K. Kawabata, K. Shiozaki, and M. Sato, Topological origin of non-Hermitian skin effects, Phys. Rev. Lett. **124**, 086801 (2020).
[28] K. Kawabata, K. Shiozaki, M. Ueda, and M. Sato, Symmetry and topology in non-Hermitian physics, Phys. Rev. X **9**, 041015 (2019).
[29] K. Zhang, Z. Yang, and C. Fang, Correspondence between winding numbers and skin modes in non-Hermitian systems, Phys. Rev. Lett. **125**, 126402 (2020).
[30] K. Yokomizo and S. Murakami, Non-Bloch band theory of non-Hermitian systems, Phys. Rev. Lett. **123**, 066404 (2019).
[31] K. Yokomizo and S. Murakami, Non-Bloch band theory in bosonic Bogoliubov–de Gennes systems, Phys. Rev. B **103**, 165123 (2021).
[32] K. Yokomizo, T. Yoda, and S. Murakami, Non-Hermitian waves in a continuous periodic model and application to photonic crystals, Phys. Rev. Res. **4**, 023089 (2022).
[33] Y.-M. Hu, Y.-Q. Huang, W.-T. Xue, and Z. Wang, Non-Bloch band theory for non-Hermitian continuum systems, Phys. Rev. B **110**, 205429 (2024).
[34] V. A. Yurovsky, A. Ben-Reuven, P. S. Julienne, and C. J. Williams, Atom loss from Bose-Einstein condensates due to Feshbach resonance, Phys. Rev. A **60**, R765 (1999).
[35] L. Li, C. H. Lee, and J. Gong, Topological switch for non-Hermitian skin effect in cold-atom systems with loss, Phys. Rev. Lett. **124**, 250402 (2020).
[36] G. Harari, M. A. Bandres, Y. Lumer, M. C. Rechtsman, Y. D. Chong, M. Khajavikhan, D. N. Christodoulides, and M. Segev, Topological insulator laser: Theory, Science **359**, eaar4003 (2018).
[37] Y. Ota, K. Takata, T. Ozawa, A. Amo, Z. Jia, B. Kante, M. Notomi, Y. Arakawa, and S. Iwamoto, Active topological photonics, Nanophotonics **9**, 547 (2020).
[38] M. A. Bandres, S. Wittek, G. Harari, M. Parto, J. Ren, M. Segev, D. N. Christodoulides, and M. Khajavikhan, Topological insulator laser: Experiments, Science **359**, eaar4005 (2018).
[39] B. Bahari, A. Ndao, F. Vallini, A. E. Amili, Y. Fainman, and B. Kanté, Nonreciprocal lasing in topological cavities of arbitrary geometries, Science **358**, 636 (2017).
[40] S. Longhi, D. Gatti, and G. D. Valle, Robust light transport in non-Hermitian photonic lattices, Sci. Rep. **5**, 13376 (2015).
[41] A. Metelmann and A. A. Clerk, Nonreciprocal photon transmission and amplification via reservoir engineering, Phys. Rev. X **5**, 021025 (2015).
[42] C. C. Wanjura, M. Brunelli, and A. Nunnenkamp, Topological framework for directional amplification in driven-dissipative cavity arrays, Nat. Commun. **11**, 3149 (2020).
[43] S. Weidemann, M. Kremer, T. Helbig, T. Hofmann, A. Stegmaier, M. Greiter, R. Thomale, and A. Szameit, Topological funneling of light, Science **368**, 311 (2020).
[44] D. Halder, R. Thomale, and S. Basu, Circuit realization of a two-orbital non-Hermitian tight-binding chain, Phys. Rev. B **109**, 115407 (2024).
[45] A. Ghatak, M. Brandenbourger, J. van Wezel, and C. Coulais, Observation of non-hermitian topology and its bulk–edge correspondence in an active mechanical metamaterial, Proc. Natl. Acad. Sci. USA **117**, 29561 (2020).
[46] A. Eichler and O. Zilberberg, *Classical and Quantum Parametric Phenomena* (Oxford University Press, Oxford, 2023).
[47] M. Soriente, T. L. Heugel, K. Omiya, R. Chitra, and O. Zilberberg, Distinctive class of dissipation-induced phase transitions and their universal characteristics, Phys. Rev. Res. **3**, 023100 (2021).
[48] C. Macklin, K. O'Brien, D. Hover, M. E. Schwartz, V. Bolkhovsky, X. Zhang, W. D. Oliver, and I. Siddiqi, A near–quantum-limited Josephson traveling-wave parametric amplifier, Science **350**, 307 (2015).
[49] M. Evans, S. Gras, P. Fritschel, J. Miller, L. Barsotti, D. Martynov, A. Brooks, D. Coyne, R. Abbott, R. X. Adhikari, *et al.*, Observation of parametric instability in advanced LIGO, Phys. Rev. Lett. **114**, 161102 (2015).
[50] A. Grimm, N. E. Frattini, S. Puri, S. O. Mundhada, S. Touzard, M. Mirrahimi, S. M. Girvin, S. Shankar, and M. H. Devoret, Stabilization and operation of a Kerr-cat qubit, Nature (London) **584**, 205 (2020).
[51] T. L. Heugel, O. Zilberberg, C. Marty, R. Chitra, and A. Eichler, Ising machines with strong bilinear coupling, Phys. Rev. Res. **4**, 013149 (2022).
[52] O. Ameye, A. Eichler, and O. Zilberberg, The parametric instability landscape of coupled Kerr parametric oscillators, Phys. Rev. Res. **7**, 033204 (2025).
[53] M. I. Dykman, C. Bruder, N. Lörch, and Y. Zhang, Interaction-induced time-symmetry breaking in driven quantum oscillators, Phys. Rev. B **98**, 195444 (2018).
[54] Y.-X. Wang and A. A. Clerk, Non-Hermitian dynamics without dissipation in quantum systems, Phys. Rev. A **99**, 063834 (2019).
[55] X. Xu, H. Xu, S. Mandal, R. Banerjee, S. Ghosh, and T. C. H. Liew, Interaction-induced double-sided skin effect in an exciton-polariton system, Phys. Rev. B **103**, 235306 (2021).
[56] J. Del Pino, J. J. Slim, and E. Verhagen, Non-Hermitian chiral phononics through optomechanically induced squeezing, Nature (London) **606**, 82 (2022).
[57] H. Lo, Y. Wang, R. Banerjee, B. Zhang, and Y. D. Chong, Switchable non-Hermitian skin effect in Bogoliubov modes, Phys. Rev. B **111**, L241401 (2025).
[58] A. McDonald, T. Pereg-Barnea, and A. A. Clerk, Phase-dependent chiral transport and effective non-Hermitian dynamics in a bosonic Kitaev-Majorana chain, Phys. Rev. X **8**, 041031 (2018).
[59] J. J. Slim, C. C. Wanjura, M. Brunelli, J. Del Pino, A. Nunnenkamp, and E. Verhagen, Optomechanical realization of the bosonic Kitaev chain, Nature (London) **627**, 767 (2024).
[60] J. H. Busnaina, Z. Shi, A. McDonald, D. Dubyna, I. Nsanzineza, J. S. Hung, C. S. Chang, A. A. Clerk, and C. M. Wilson, Quan-

tum simulation of the bosonic Kitaev chain, Nat. Commun. **15**, 3065 (2024).

[61] L.-L. Wan and X.-Y. Lü, Quantum-squeezing-induced point-gap topology and skin effect, Phys. Rev. Lett. **130**, 203605 (2023).

[62] B. Schneider, A. Dikopoltsev, M. Bestler, P. Täschler, M. Beck, D. Burghoff, O. Zilberberg, and J. Faist, Ultrafast non-Hermitian skin effect, arXiv:2505.03658.

[63] P. Fulde and R. A. Ferrell, Superconductivity in a strong spin-exchange field, Phys. Rev. **135**, A550 (1964).

[64] M. wen Xiao, Theory of transformation for the diagonalization of quadratic Hamiltonians, arXiv:0908.0787.

[65] A. Gardin, G. Bourcin, C. Person, C. Fumeaux, R. Lebrun, I. Boventer, G. C. Tettamanzi, and V. Castel, Level attraction from interference in a two-tone-driven cavity magnonics system, Phys. Rev. Appl. **23**, 014048 (2025).

[66] Ş. K. Özdemir, S. Rotter, F. Nori, and L. Yang, Parity–time symmetry and exceptional points in photonics, Nat. Mater. **18**, 783 (2019).

[67] See Supplemental Material at http://link.aps.org/supplemental/10.1103/yhkx-tn6l for details on the Bogoliubov diagonalization for our model, for the derivation of the mean-field von Neumann equation, on the application of non-Bloch theory for our model, on experimental realizations, and on the discretized limit of our model, which includes Refs. [73–76].

[68] J. Y. Lee, J. Ahn, H. Zhou, and A. Vishwanath, Topological correspondence between Hermitian and non-Hermitian systems: Anomalous dynamics, Phys. Rev. Lett. **123**, 206404 (2019).

[69] N. Okuma and M. Sato, Quantum anomaly, non-Hermitian skin effects, and entanglement entropy in open systems, Phys. Rev. B **103**, 085428 (2021).

[70] M. G. Silveirinha, Chern invariants for continuous media, Phys. Rev. B **92**, 125153 (2015).

[71] T. Uto and D. Oue, Parametric instability in a magnomechanical system, Phys. Rev. B **112**, 024305 (2025).

[72] F. Claude, M. J. Jacquet, Q. Glorieux, M. Wouters, E. Giacobino, I. Carusotto, and A. Bramati, Observation of the diffusive Nambu–Goldstone mode of a non-equilibrium phase transition, Nat. Phys. **21**, 924 (2025).

[73] R. Rossignoli and A. M. Kowalski, Complex modes in unstable quadratic bosonic forms, Phys. Rev. A **72**, 032101 (2005).

[74] D. C. Brody, Biorthogonal quantum mechanics, J. Phys. A: Math. Theor. **47**, 035305 (2014).

[75] M. Wouters and I. Carusotto, Excitations in a nonequilibrium Bose-Einstein condensate of exciton polaritons, Phys. Rev. Lett. **99**, 140402 (2007).

[76] D. Burghoff, Unraveling the origin of frequency modulated combs using active cavity mean-field theory, Optica **7**, 1781 (2020).